Journal of Power Sources 516 (2021) 230680

Contents lists available at ScienceDirect

Journal of Power Sources

journal homepage: www.elsevier.com/locate/jpowsour

Thermal management evaluation of Li-ion battery employing multiple phase change materials integrated thin heat sinks for hybrid electric vehicles

Abubakar Gambo Mohammed [a], Karem Elsayed Elfeky [a,b,*], Qiuwang Wang [a]

[a] Key Laboratory of Thermo-Fluid Science and Engineering, Ministry of Education, School of Energy and Power Engineering, Xi'an Jiaotong University, Xi'an, Shaanxi, 710049, PR China
[b] Mechanical Engineering Department, Benha Faculty of Engineering, Benha University, Egypt

HIGHLIGHTS

- Multiple PCMs incorporated thin heat sinks for battery thermal management is proposed.
- The thermal performance of the battery based on maximum temperature upsurge is investigated.
- The distributions of PCMs based on melting point and latent heat were carefully explored.
- The optimal design for the distribution of PCMs is obtained for the proposed battery.

ARTICLE INFO

Keywords:
Lithium-ion battery
Battery thermal management
Phase change materials
Temperature upsurge
Temperature homogenization

ABSTRACT

The optimal performance of a Li-ion battery is directly impacted by temperature. In order to control the temperature rise and provide even temperature distributions in the battery pack, a thermal management scheme comprises thin heat sinks with multiple phase change materials (PCMs) and air channels is investigated in this paper. The cooling performance and temperature homogenization of the battery thermal management (BTM) system are carefully studied under various configurations of PCMs. The results show that increasing the air inlet velocity has less effect in suppressing the temperature rise at early discharge stage, but ameliorates as the discharge prolonged to 3600 s. The standard deviation of the temperature (STDV) and maximum temperature of the batteries can be decreased by arranging PCMs with a lower melting temperature at the midsection and a higher melting temperature at the air outlet region of the heat sinks. In addition, for volume fraction of PCMs, Case IV, having a PCM with a higher melting point adjacent to the air outlet region and occupying one-half the height of the heat sink, illustrates a lower temperature rise and decreases the maximum temperature in the battery module by 1.024 K, 2.186 K, and 2.553 K, compared to Case I, II, and III, respectively.

1. Introduction

The imminent world energy policy intensified pressure on development of less or zero emission vehicles in order to reduce greenhouse gas and pollutant emissions. Meanwhile, the carbon emission recorded in the year 2018 raised up to 2% compared to the emission in the last seven years, which has a direct correlation with the increase in passenger cars in the world [1]. The conversion of transport sector from gasoline consuming vehicles to electric vehicles (EVs) and plug-in hybrid electric vehicles (PHEV) can aids in reducing greenhouse gas emission up to 20%, and even a 40% more reduction if the electric power generated originates from renewable sources [2]. Lithium-ion battery is recognized as a promising alternative for energy storage and power source for clean energy vehicles [3] and off-grid power supply [4], due to its high energy density, and long cycle life. However, the performance of Li-ion battery is directly impacted by temperature [5], which, at low temperature give rise to comparatively poor performance and probably a thermal runaway at high temperature. An improper operating temperature of the battery will increase the impedance, aging, and capacity fading [6,7].

* Corresponding author. Key Laboratory of Thermo-Fluid Science and Engineering, Ministry of Education, School of Energy and Power Engineering, Xi'an Jiaotong University, Xi'an, Shaanxi, 710049, PR China.
E-mail address: karem_elfeky@xjtu.edu.cn (K.E. Elfeky).

https://doi.org/10.1016/j.jpowsour.2021.230680
Received 27 February 2021; Received in revised form 8 October 2021; Accepted 24 October 2021
Available online 30 October 2021
0378-7753/

Nomenclature

ρ	Density [kg•m^{-3}]
c_p	Specific heat capacity [J•kg^{-1}•K^{-1}]
T	Temperature [K]
Q	Battery heat generation [W]
k	Thermal conductivity [W•m^{-1}•K^{-1}]
H	Total enthalpy of PCM [J•m^{-3}]
β	Liquid phase fraction
γ	Latent heat of PCM [J•m^{-3}]
P	Static pressure [Pa]
$\vec{v}$	Velocity vector [m•s^{-1}]

Subscripts

a	air
b	battery
be	bottom edge
g	generation
l	liquid phase
$melt$	melting
ref	reference value
s	Solid phase
te	top edge

Acronyms

BTM	Battery thermal management
CFD	Computational fluid dynamics
D	Design
EV	Electric vehicle
PHEV	Plug-in hybrid electric vehicle
PCM	Phase change material

Thus, in order to maintain the optimum performance and similarly reflect safety risks, an appropriate battery thermal management (BTM) system which has capability and system reliability, less weight, and low parasitic power consumption is essential. The desired operation temperature for a Li-ion battery should be between 25 and 50 °C, with a temperature gradient below 5 °C [8–10].

For the last decades, various techniques have been investigated for battery thermal management which includes passive, active, and hybrid system. The passive BTM system may use natural air convection, phase change material (PCM), or heat pipe. While, the active system makes use of forced air convection or liquid (water, oil, or refrigerant) circulation in the battery module. The hybrid BTM system combined two or more passive and active systems. Each cooling system has advantages and drawbacks. The natural air cooling solution is simple, straightforward, and does not require any extra equipment. However, natural convection cannot be enough to dissipate abundant heat generated in the battery module especially for high power batteries operating at high ambient temperature. Also, it provides large uneven temperature beyond the acceptable limit due to its low thermal conductivity [11]. Thus, natural air cooling is unacceptable for BTM. The active air cooling is achieved by blowing air on batteries surfaces or through battery module/pack in order to take away the excess heat [12–16]. It is also simple, but due to its poor thermal capacity and thermal conductivity, forced air cooling may not be sufficient to remove heat from battery module/pack under abuse condition. Likewise, the uneven temperature distribution within the battery module/pack is unavoidable. Moreover, the maintenance is easy, has low cost, but low efficiency. As air cooling using natural or forced convection could not sufficiently dissipate heat and provide even temperature distribution in a battery pack, numerous studies proposed cooling of battery module/pack using liquid [17–19]. Compared with air, liquid has higher heat capacity and thermal conductivity and can provide better thermal performance and uniform temperature distribution. Nevertheless, it occupies more space, increases complexity, weight and cost [20]. Another critical issue is liquid leakage, its maintenance is difficult and consume more power. The heat pipe-based BTM system works via transfer of heat between solid interfaces by taking advantages of phase transition and thermal conductivity of the working fluid [21]. The vapor moves from evaporator section to condenser as a result of vapor pressure difference, however, the fluid in the condenser flows back to evaporator due to the driven forces, like capillary and gravitational forces [22–25]. The heat pipe based BTM is expensive and may not provide a desire uniform temperature.

Contrast to active cooling, passive cooling using phase change material (PCM) is simple and does not require extra power parasitic components such as fan/blower, pump, pipes, and chiller. It provide quick temperature response, efficient suppress of temperature upsurge, and temperature uniformity by absorbing and storing heat during phase transition. For the past two decades, numerous works have been conducted for PCM-based BTM scheme [26–29]. The PCM-based BTM has high efficiency, low cost, and easy maintenance. However, low thermal conductivity limits its widespread applications. Volume expansion and possibly liquid leakage after melting are also challenging [30]. To overcome the low thermal conductivity limitation and leakage problem, several approaches have been conducted to make composite PCMs. This is achieved by adding thermal conductive enhancers such as carbon-based additives [31–33], and metal foam/matrix [34–36]. In hybrid BTM system, PCM-based thermal management is commonly combine with passive or active systems such as PCM/forced air convection, PCM/liquid circulation, or PCM with heat pipes. In PCM-based hybrid thermal management scheme, the sensible and latent heat capacity of the PCM play the vital role while, active thermal management usually aids in cooling the PCM [37]. Compare with conventional BTM system, the hybrid system provides better thermal performance specifically under stressful and abuse operation conditions than any passive or active thermal management alone.

The issue of BTM with multi-PCM layers received less attention and few studies conducted in this regard can be found in literature. In an effort to examine the thermal performance and minimize cost and size of BTM system, Ramandi et al. [38] compared single and double series PCM layers around a prismatic battery numerically. They reported that, the double PCM shells configuration outperformed the single shell configuration based on temperature control and exergy efficiency. Furthermore, increasing the ambient temperature for the non-insulated cases studied, the exergy efficiency decreases while the destroyed exergy rises steadily. Al-Hallaj and Albright [39] proposed a system combining two PCMs with different melting temperatures in order to control the temperature at a desired range for batteries thermal management. The inner PCM next to the batteries is designed to have higher melting temperature than the outer PCM, but lower meting point than the allowable batteries temperature. The heat generated from the batteries will be absorbed by the inner PCM and then dissipated to the outer PCM. The temperature difference between the two PCMs can probably enhanced heat transfer by conduction between the two PCMs. Lin et al. [40] analyzed the influence of different parameters such as phase change temperature, and thermal conductivity on prismatic Li-ion battery surrounded by two PCM shells. Zhao et al. [41] considered melting temperature, thermal conductivity and PCM distribution to relatively investigate the thermal performance of thin heat sink integrated with PCM for battery thermal management system. Four different melting temperature and latent heat of PCMs were employed alongside the heat sink. Their simulation results illustrated that, the maximum temperature and temperature difference can remarkably be decrease by increasing

the latent heat and reducing the melting temperature values. The thermal conductivity has negligible influence for a thinner PCM layer. Dispersal of PCM in thin heat sink having different latent heat and melting temperature clearly have impact on temperature uniformity and maximum temperature rise.

Based on the aforementioned, the passive multiple PCM-based combining active air-based thermal management lack detailed parametric analysis in the literature, to consider systematically the effect of PCMs arrangement according to their latent heat and melting temperature. In this paper, a hybrid BTM system incorporated multiple PCMs with mini heat sink is introduced with the aim of optimizing the thermal management of Li-ion battery pack inspired by the works of Fan et al. [42] and Zhao et al. [41]. Two dimensional transient thermal analysis of multi-PCMs with mini air channels were carried out. The impact of PCMs configurations, and PCMs volume fraction design were carefully explored. Crucial indicators from the simulation results such as maximum temperature rise, temperature difference and standard deviation of the temperature field (STDV) of the battery module were presented.

2. Model setup

The Li-ion battery pack designed for PHEV containing eight prismatic cells and being discharged under stressful power profile of 1.3 × US06 (PHEV40) is considered [42]. The thermophysical properties and dimensions of the 15-Ah cell are presented in Table 1. The heat generation rates of 28,000 Wm^{-3} was assumed under 1.3 × US06 (PHEV40) power profiles and the module is expected to operate for 600 s drive cycle. Fig. 1(a) illustrated the schematic of the battery thermal management system. The battery module consist of eight prismatic cells and nine heat sinks. In order to simplify the computations, and save time and cost, two dimensional model of the battery module was considered. The gap spacing between the adjacent cells were maintained at 3 mm, in which 1 mm thick PCMs were attached at the surface of each cell with 1 mm mini air channel in between as shown in Fig. 1 (b). The height of the heatsink is divided into three equal sections each filled with different PCMs. The air passage including inlet and outlet, the PCM 1, PCM 2, and PCM 3, and the batteries were also illustrated. Different designs of PCMs distribution were tabulated in Table 2. In each design, the PCMs arrangement is considered starting from the bottom (adjacent to the air inlet) to the top (adjacent to the air outlet) of the battery module. For instance, in design 1 (DI), PCM 1 is placed at the bottom, PCM 2 at the midsection, and PCM 3 at the top part, which is summarized as PCM 1-2-3. To select a PCM for BTM, two important parameters such as latent heat and melting temperature should be considered. In order to achieve effective heat dissipation and uniform temperature distribution in the entire battery module, PCM with melting point below 45 °C should be chosen to maintain the maximum temperature below 50 °C [43]. The specifications of the selected PCMs used in this work are summarized in Table 3. Moreover, to further optimize the thermal performance of the proposed system, four different cases for the PCMs volume fraction were investigated systematically as depicted in Table 4. The height of the heat sink is divided into three unequal sections and filled with different PCMs as shown in Fig. 1(c).

Table 1
Properties and dimension of the prismatic cells [42].

Properties/dimension	Value
Active area dimensions (mm)	6 × 145 × 255
Density ($kg•m^{-3}$)	2335
Specific heat capacity ($J•kg^{-1}•K^{-1}$)	745
Thermal conductivity ($W•m^{-1}•K^{-1}$)	27 (along surface) 0.8 (in thickness direction)

3. Numerical solution

3.1. Mathematical model and boundary conditions

Generally, in Li-ion battery the heat released via electrochemical reaction and Joule effect are the two primary heat sources. For a constant discharge rate, uniform heat generations is presumed inside the cell. The generated heat within the cell will then be absorbed by the PCM through conduction and the forced air circulation assists in cooling the PCM. Based on finite volume method, numerical simulations were carried out to investigate the thermal behavior of the cells. The commercial CFD package (FLUENT 17.2) was employed to discretized and solve the governing conservation equations.

The conjugate heat transfer scheme is adopted for the stated problem. Adiabatic boundary condition was chosen for the whole surfaces except the velocity inlet and outlet which were taken as inlet and outflow boundary conditions, respectively. The governing energy equation of the battery is given as:

$$\rho_b C_{p,b}\frac{\partial T_b}{\partial t} = \nabla(k_b \nabla T_b) + Q_g \tag{1}$$

where ρ_b, C_{pb}, T_b, and k_b are the density, specific heat capacity, temperature, and thermal conductivity of the battery, respectively. The Q_g represents the generated heat in the battery.

The enthalpy-porosity method is adopted to treat the liquid/solid phase change during the PCM melting process. For the phase transition of PCM, the energy equation is given as follows:

$$\rho\frac{\partial H}{\partial t} = k\left(\frac{\partial^2 T}{\partial x^2} + \frac{\partial^2 T}{\partial y^2}\right) + S \tag{2}$$

$$H = H_o + \Delta H \tag{3}$$

$$H_o = H_{ref} + \int_{T_{ref}}^{T} C_{p,PCM}\, dT \tag{4}$$

$$\Delta H = \beta\gamma \tag{5}$$

$$\beta = \begin{cases} 0 & T < T_s \\ \dfrac{T - T_s}{T_l - T_s} & T_s < T < T_l \\ 1 & T > T_l \end{cases} \tag{6}$$

where H, T, and S symbolize the total enthalpy, temperature, and source term of the PCM, respectively. H_o represents the sensible enthalpy, and ΔH denotes the latent heat content which changes between solidification and γ (melting). The H_{ref}, $C_{p,PCM}$, β, T_s, and T_l are the specific enthalpy at reference temperature, specific heat capacity of PCM at constant pressure, liquid fraction, solidus temperature, and liquidus temperature, respectively.

For the air flow in the mini-channels, a laminar flow was considered entering each air channel and the governing conservation equations are as follows:

$$\frac{\partial \rho_a}{\partial t} + \nabla(\rho_a \vec{v}) = 0 \tag{7}$$

$$\rho_a\frac{\partial(\vec{v})}{\partial t} + \nabla\left(\rho_a \vec{v}\cdot\vec{v}\right) = -\nabla P \tag{8}$$

$$\rho_a C_{p,a}\frac{\partial T_a}{\partial t} = \nabla(k_a \nabla T_a) \tag{9}$$

where, ρ_a, P, $C_{p,a}$, k_a, T_a, and $\vec{v}$ are the density, static pressure, heat capacity, thermal conductivity, air temperature, and velocity vector of

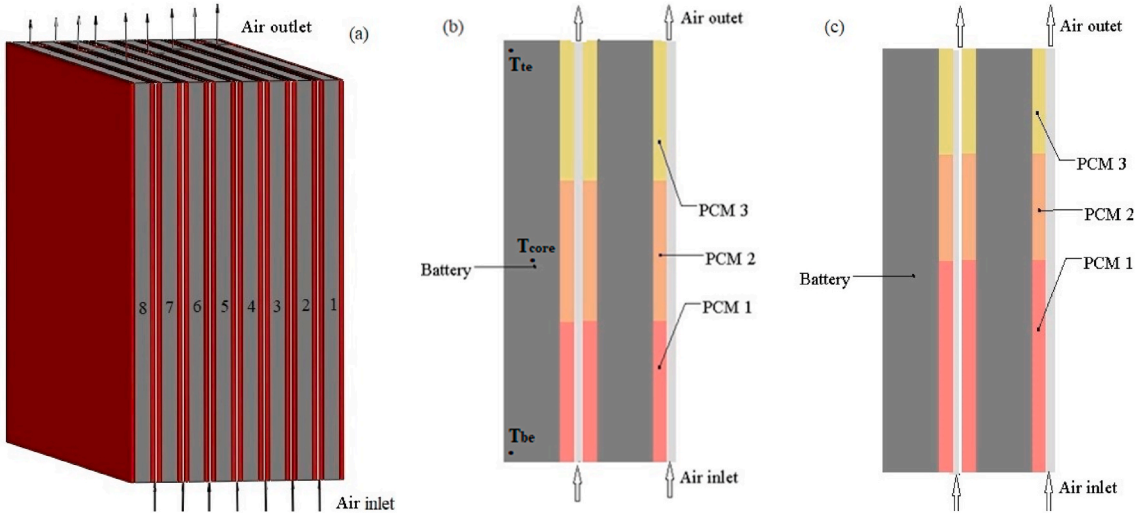

Fig. 1. Schematic of the battery module showing (a) complete module with the battery units, (b) simplified module with three equally distributed PCMs, and (c) module with three unequally distributed PCMs.

Table 2
PCMs distribution schemes.

Design	PCMs arrangement (bottom-up)	Short form
DI	PCM 1 – PCM 2 – PCM 3	PCM 1-2-3
DII	PCM 1 – PCM 3 – PCM 2	PCM 1-3-2
DIII	PCM 2 – PCM 1 – PCM 3	PCM 2-1-3
DIV	PCM 2 – PCM 3 – PCM 1	PCM 2-3-1
DV	PCM 3 – PCM 1 – PCM 2	PCM 3-1-2
DVI	PCM 3 – PCM 2 – PCM 1	PCM 3-2-1

Table 3
Specifications of the selected PCMs [44].

	PCM 1	PCM 2	PCM 3
Melting temperature range (°C)	34–36	29–36	27–33
Main peak melting (°C)[a]	35	33	31
Heat of fusion (kJ•kg^{-1})	240	160	165
Specific heat (kJ•kg^{-1}•K^{-1})	2	2	2
Density solid/liquid (kg•m^{-3})	880/770	860/770	880/760
Thermal conductivity (W•m^{-1}•K^{-1})	0.2	0.2	0.2

[a] Values adopted in the simulations.

Table 4
PCMs volume fraction according to the height (*H*) of the heat sink.

Case	Bottom PCM	Middle PCM	Top PCM
I	H/3	H/3	H/3
II	H/2	H/4	H/4
III	H/4	H/2	H/4
IV	H/4	H/4	H/2

the air, respectively.

The pressure based, and second order transient model was employed. The SIMPLE algorithm was adopted to handle the velocity-pressure coupling. The iteration convergence was set whereby the residuals for the governing equations for flow was 10^{-5} and for thermal energy was 10^{-7}. The time step was 1 s, and the iterations per time step was set to be 60 to assured that the computation converged in each and every time step. The assumptions uphold in the simulations are as follows. The thermophysical properties are constant and isotropic except the thermal conductivity. An orthotropic thermal conductivity was considered for the cells. The initial temperature of the module and ambient temperature are the same (27 °C). The volume change and fluid flow of the PCM were not considered. The radiation effect is also neglected.

3.2. Grid independence verification

To validate the numerical solution, grid independence tests were carried out under 0.227 m/s and 300 K flow rate and inlet temperature, respectively. Three different grids were generated consisting 15,895, 52,700 and 112,453 cells. The maximum battery temperature and outlet air temperature are chosen for convergence criteria. As shown in Table 5, the maximum difference among the results is below 0.012%. Therefore, the midium grid (52,700 cells) is selected in this study. In addition, the current work is validated with the numerical results obtained by Fan et al. [42]. The effect of gap spacing between the cells is considered with air flow rate at 20.4 m^3/h after 600 s discharge time.

Fig. 2 compared the STDV of the temperature field in the battery module at the end of 600 s discharge time predicted in this work and in Ref. [42].

4. Results and discussion

To begin with, preliminary studies were carried out to assess the thermal performance of the battery module whereby, a single PCM configuration (as a benchmark) is compared with that of multiple PCMs configurations as depicted in Fig. 3. The dash, dot, and dash-dot lines signify the benchmark configuration with only PCM 1, PCM 2, and PCM 3, respectively. The connected solid lines with symbols denoted multiple PCMs arrangement (see Table 2). It can be seen that, the single and multiple PCMs configurations have different variation trends in temperature rise. The graphs of the benchmark configurations can distinctly be noticed having sharp curves prior, during and after melting of the PCM. At early discharge process, the single PCM 1 and PCM 2 designs exhibited higher temperature rise among the rest of the configurations. Comparing to single PCM 1 design, the PCM 1-3-2 and PCM 2-3-1 schemes for example, decreased the maximum temperature each by 3.1 K at 600 s. This can probably be attributed to the high melting point of the PCM 1 that takes time before it started absorbing the heat from the battery surface. Likewise, the PCM 1-3-2 and PCM 2-3-1 configurations successfully decreased the maximum temperature upsurge by 1.3 K compared to the sole PCM 2 design. The single PCM 3 scheme demonstrated the lowest temperature rise until 2450 s, however, it suffers the worst thermal status together with PCM 2 scheme at the end of the discharge process. Contrary to a single PCM configuration, the multiple PCMs modules illustrated mild temperature upsurge both at the

Table 5
Grid independence tests for design I (DI) under 0.227 m/s and 300 K.

Flow time (s)	Battery maximum temperature (K)				Outlet air temperature (K)			
	15,895 cells	52,700 cells	112,453 cells	Max diff. (%)	15,895 cells	52,700 cells	112,453 cells	Max diff. (%)
600	305.401	305.369	305.377	0.010	305.341	305.309	305.317	0.010
3600	316.662	316.661	316.660	0.001	316.471	316.493	316.487	0.007

The trend of standard deviation in this study portrayed good agreement with that in Ref. [42], having a maximum deviation of 4.5% error, which signifies that the established model is practically reliable.

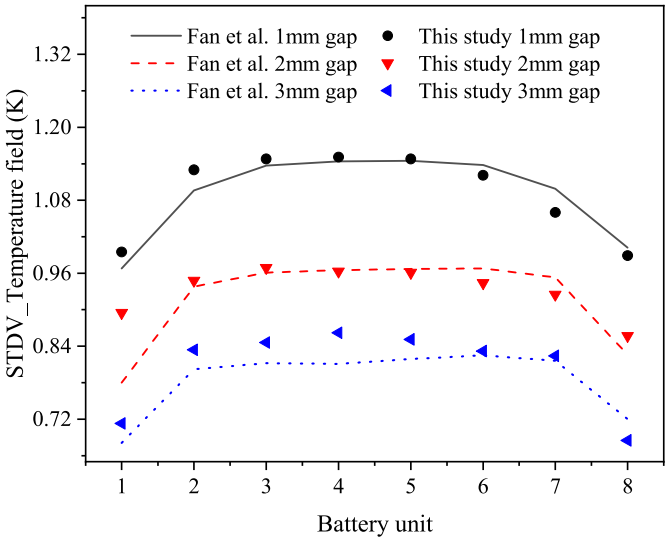

Fig. 2. Results comparison of STDV of temperature field within the batteries at $t = 600$ s.

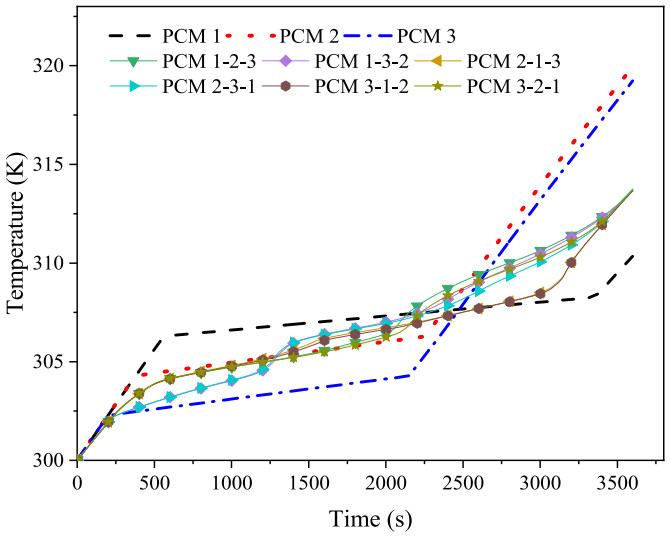

Fig. 3. Temperature profile of single PCM and multiple PCMs configurations.

beginning and end of the discharge. The multiple PCMs arrangements effectively suppressed the rapid temperature rise by at least 6.0 K compared to the individual PCM 2 and PCM 3 scheme at 3600 s. Whereas, the PCM 1 outperformed multiple PCMs designs in reducing the temperature rise by at least 3.2 K at 3600 s. Thus, it can be worth noting that multi-PCMs configurations in a battery module incorporated with force air convection, can remarkably control the temperature rise at a desired range both at early and later discharge process.

4.1. Effect of air inlet velocity

In this section, the thermal behavior of the proposed battery module was further assessed by considering different air inlet velocities. Based on the assumptions that the corresponding values of the Reynold numbers (Re = 370, 800, 1230, 1660, and 2090) entering the air channels were in laminar phase and distributed evenly [42], the temperature profile of the module is presented in Fig. 4.

The design DIV (PCM 2-3-1), meaning that PCM 2 placed at the bottom section, PCM 3 at the midsection, and PCM 1 at the top region is employed. As illustrated in Fig. 4 (a), increasing the inlet velocity decreases the temperature rise, which can clearly be distinct after 2000 s of discharge. At early discharge stage, that is before the PCMs completely melted, the inlet air velocity has minimal effect on mitigating the temperature rise. Moreover, the temperature difference (ΔT) within the battery is evaluated and presented in Fig. 4 (b) and (c). Two extreme positions were considered T_{core} - T_{te} (Fig. 4(a)), and T_{core} - T_{be} (Fig. 4(b)). Initially, the value of ΔT drops below zero in both Fig. 4(a) and (b) and then rise as the discharge prolonged. Increasing the air inlet velocity minimizes the temperature values (Fig. 4(a)), which is contrary to Fig. 4 (c). At early discharge stage, the temperature at the core (T_{core}) of the batteries were lower than at the two extreme points (T_{te} and T_{be}). The reason is that the PCM having lower melting point (PCM 3) among the three PCMs is situated at the midsection of the battery module and thus, it first absorbed the heat during phase transition.

Consequently, its thermal function triggered and started melting by absorbing the excess heat from the batteries at that region prior to the remaining PCMs. However, the temperature difference in both the two cases are well below the recommended limit (5 °C). The medium value of the Reynold numbers (Re = 1230), which is equivalent to 0.124 m/s of the inlet velocity is thus selected for the subsequent analysis based on trade-off between the maximum temperature rise, temperature uniformity, and fan power requirement.

4.2. Constant T_{melt}, different latent heat and vice-versa

To better understand the thermal performance of the proposed BTM, we also analyze the thermal effectiveness of the battery module based on assumptions that, maintaining a similar melting temperature (T_{melt}) of the three PCMs and varying the latent heat, and vice-versa. The air inlet velocity and temperature were considered to be 0.124 m/s and 300 K, respectively.

4.2.1. Evolution of temperature control based on constant T_{melt}, different latent heat

Fig. 5 (a) and (b) depict the maximum temperature upsurge and the STDV of the temperature within the individual batteries after 600 s discharged, respectively. It can be seen that, the configurations having lower latent heat at the bottom (adjacent to the air entrance) side and higher latent heat at the top (adjacent to the air outlet) part of the battery module exhibited lower temperature rise and better even temperature distribution compared to the remaining four configurations.

This can be explain as follows. As the PCM absorbed and stored the generated heat from the battery, the cooling air drives in and dissipates the excess heat out of the battery module. The air entered from the bottom to the top section of the battery module becomes hot as it passes

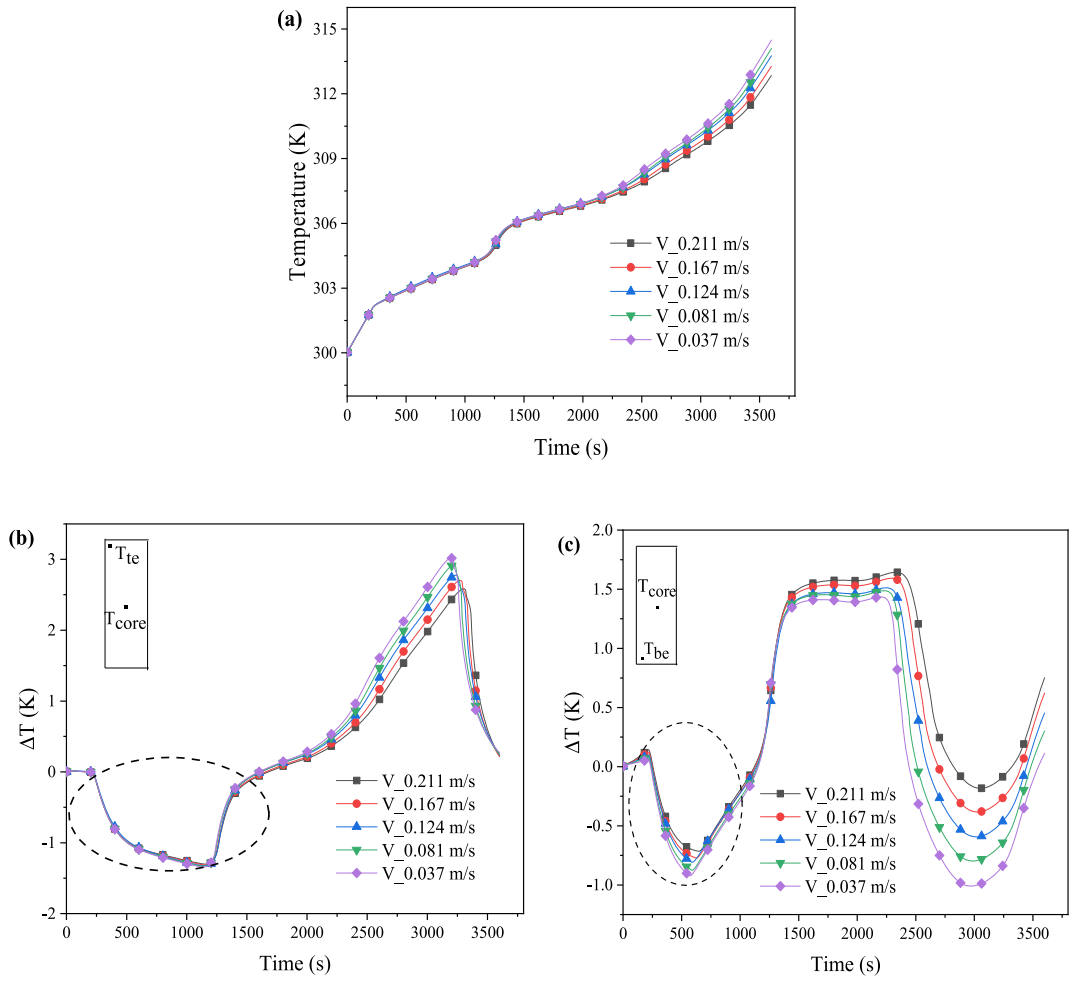

Fig. 4. Evolution of (a) maximum temperature, (b) temperature gradient between T_{core} and ${}_{a}T_{te}$, and (c) temperature gradient between T_{core} and ${}_{b}T_{be}$ under different air inlet velocity (DIV selected).

through the mini-channel. Thus, the PCM adjacent to the air outlet absorbed extra heat from the passing air. The PCM with lower latent heat can probably melt and exhausted its heat of fusion prior to the end of discharge, which will directly affect the thermal performance of the batteries. Whereas, the PCM with higher latent heat at the outlet region can take advantage of its latent heat to absorbs the excess heat and control the temperature rise at that region.

Thus, for multiple PCMs distribution integrated with air passages, placing PCMs with higher latent heat at the outlet regions will outperform other configurations in terms of lowering the temperature and providing temperature uniformity in the battery module.

However, as the discharge period prolonged to 3600 s, the configurations having higher latent heat at the midsections and outlet regions of the battery module illustrated almost similar performance with lower temperature upsurge compared to the arrangements with lower latent heat at the outlet zones, as shown in Fig. 5 (c). In contrast to the temperature profile at the end of 600 s discharge (Fig. 5 (a)), the temperature in the module toward battery unit 8 increased (Fig. 5 (c)), indicating that the air flow rates differed at the individual air-channels regardless of the uniform given values in the simulations. This similar phenomenon was also observed by Fan et al. [42]. Likewise, for the temperature uniformity in the module, the PCMs arrangement with higher latent heat at the outlet regions again demonstrates better thermal performance portraying minimum values of STDV at the end of 3600 s discharge.

4.2.2. *Evolution of temperature control based on constant latent heat, different T_{melt}*

Now, maintaining a similar latent heat (165 kJ/kg) for the three PCMs and varying their melting point, the thermal behavior of the individual cells are illustrated in Fig. 6. The maximum temperature and STDV of the temperature field after 600 s discharged are shown in Fig. 6 (a) and (b), respectively. As shown, the PCMs arrangement with lower melting temperature at the midsection of the battery module (308-304-306) K exhibits low temperature rise compared to the remaining configurations. The maximum temperature upsurge was lowered by 1.14 K, and simultaneously improved temperature uniformity by 0.52 K. The reason behind that could be, at early stage of discharge, the PCM situated at the middle began melting by absorbing abundant heat from the batteries which supresses the temperature rise in the battery module. That also yields a favorable temperature uniformity as illustrated in Fig. 6 (b).

However, as the discharge period prolonged and the PCMs at all regions melted and exhausted their latent heat, the PCM configuration having higher melting point at the outlet zones (304-306-308) K demonstrated better thermal performance by lowering the maximum temperature rise by 0.3 K as depicted in Fig. 6 (c). The reason behind this phenomenon is similar to that explained in section 4.2.1.

4.3. *Thermal performance of different PCMs configurations*

To further understand the thermal effectiveness of the proposed BTM with multiple PCMs, different design of PCMs distribution (see Table 2)

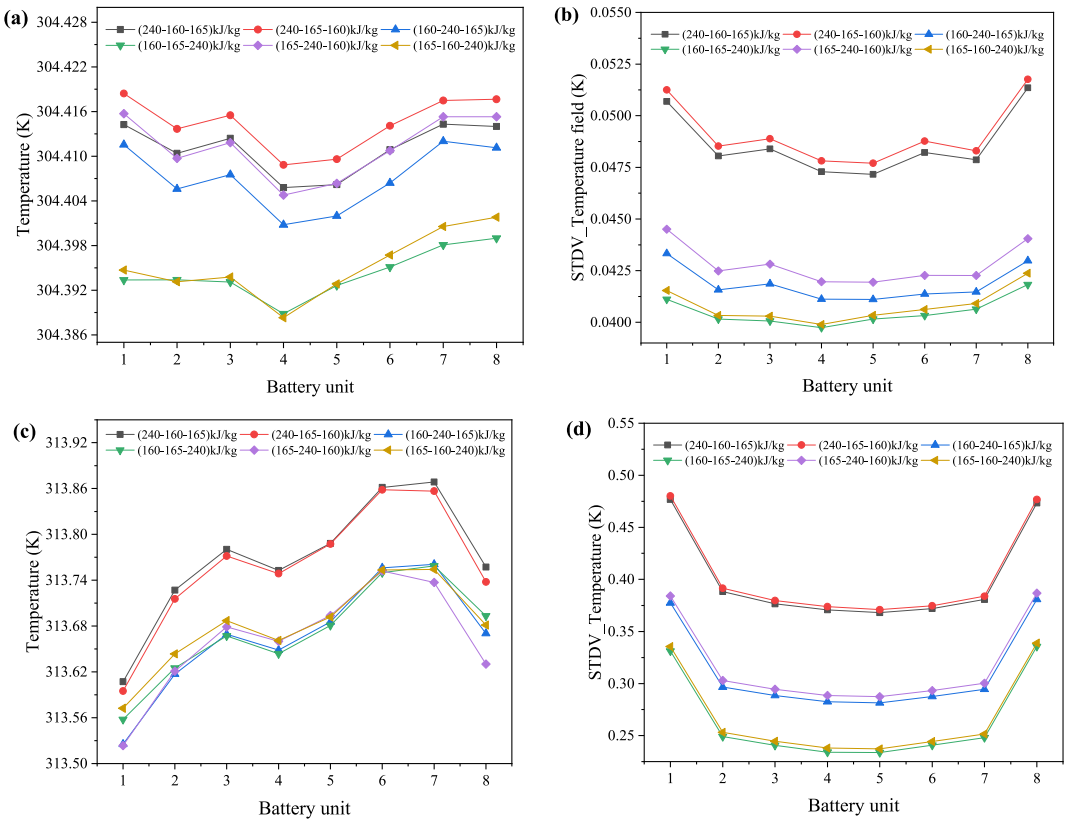

Fig. 5. Maximum temperature rise and STDV of the temperature field for the individual cells at 600 s (a, b), and 3600 s (c, d) under $T_{melt} = 306$ K, and v = 0.124 m/s.

were analyzed comprehensively. The air inlet velocity and temperature were maintained at 0.124 m/s and 300 K, respectively. Fig. 7 (a) and (b) present the maximum temperature and STDV of the temperature field within the individual battery units after 600 s. It is clear from the graphs that, assembling the PCMs according to their melting temperature and latent heat have impact on the temperature rise and temperature uniformity in the battery module.

Design DVI (PCM 3-2-1) illustrated the worst scenario among the six configurations with a maximum temperature of 305.263 K, followed by design DI with a maximum temperature of 304.998 K at 600s discharge duration. Both designs have PCM 2 at the midsection. On the other hand, design DII (PCM 1-3-2) ameliorated the thermal performance having a maximum temperature rise of 304.181 K, followed by design DIV (PCM 2-3-1) with a maximum temperature of 304.295 K. The two designs (DII and DIV) have PCM 3 at the midsection. Designs DIII and DV exhibited an intermediate thermal performance with design DIII displaying a lower temperature rise followed by design DV. Both configurations have PCM 1 at the midsection of the battery module.

Another critical parameter to assess the battery thermal management system is the uniform temperature distribution in the battery module/pack as it directly impact the battery life. Fig. 7 (b) presents the STDV of the temperature fields for the eight battery units at 600 s discharge duration. Design DII and DIV demonstrated superior uniform temperature distribution compared to the other four designs. They succeeded in improving the temperature uniformity by an average of 57%. It is worth noting that, among the PCMs arrangement discussed, designs DII and DIV illustrated better performance by supressing the temperature rise and improving temperature uniformity after 600 s of discharge. Both designs have PCM 3 at the middle of the PCMs distribution, which has the lowest melting temperature among the three PCMs.

As the discharge time extended to 3600 s, design DII which illustrated better thermal performance at 600 s turn out to be the second worst among the remaining configuration with a maximum temperature rise of 314.761 K after 3600 s. Designs DIV and DVI (both having PCM 1 at the outlet zones) exhibited lower temperature rise and provided better temperature uniformity as depicted in Fig. 7 (c) and (d), respectively. They decreased the maximum temperature in the battery module by 1.03 K. In regard to even temperature distribution, design DIV increases the temperature uniformity in the battery module by 18%, 65.8%, 67.7%, 88.6%, and 89.4% compared to design DVI, DV, DIII, DII, and DI, respectively.

Fig. 7 (e) and (f) illustrated the air outlet temperature for the nine mini-channels at different discharge intervals. It was observed that the air outlet temperature depends exclusively on the PCM placed adjacent to the air exit zone. The designs DI and DIII which overlap one another presented lower temperature rise compared to the remaining configurations at 600 s as shown in Fig. 7 (e). Both designs have PCMs with lowest melting point (PCM 3) at the air outlet regions. Contrary to design DI or DIII, design DVI having a PCM with highest melting point (PCM 1) at air exit region demonstrated higher temperature rise followed by design DIV (also with PCM 1 at air outlet zone). These results corresponded reasonably with the contour of temperature in Fig. 7 (g). However, at 3600 s discharge intervals, the DVI exhibits lower temperature profile followed by DIV. Again, DVI and DIV both have PCM with higher melting point (PCM 1) at the air outlet sections. Likewise, the configurations having PCMs with higher melting point (PCM 1) at the air entrance portrayed higher temperature profile than the remaining designs. This phenomenal observation is in line with the preceding discussions. It can be concluded that considering the earlier (600 s) and later (3600 s) discharge durations, design DIV (PCM 2-3-1) exhibited optimal thermal performance in terms of mitigating the maximum temperature rise and temperature uniformity in the battery module.

And if a battery thermal designer intends to achieve temperature uniformity and low temperature rise within a battery module integrated with multiple PCMs and air channels, design DIV should be the best choice. Thus, design DIV is selected and employed in the simulations for

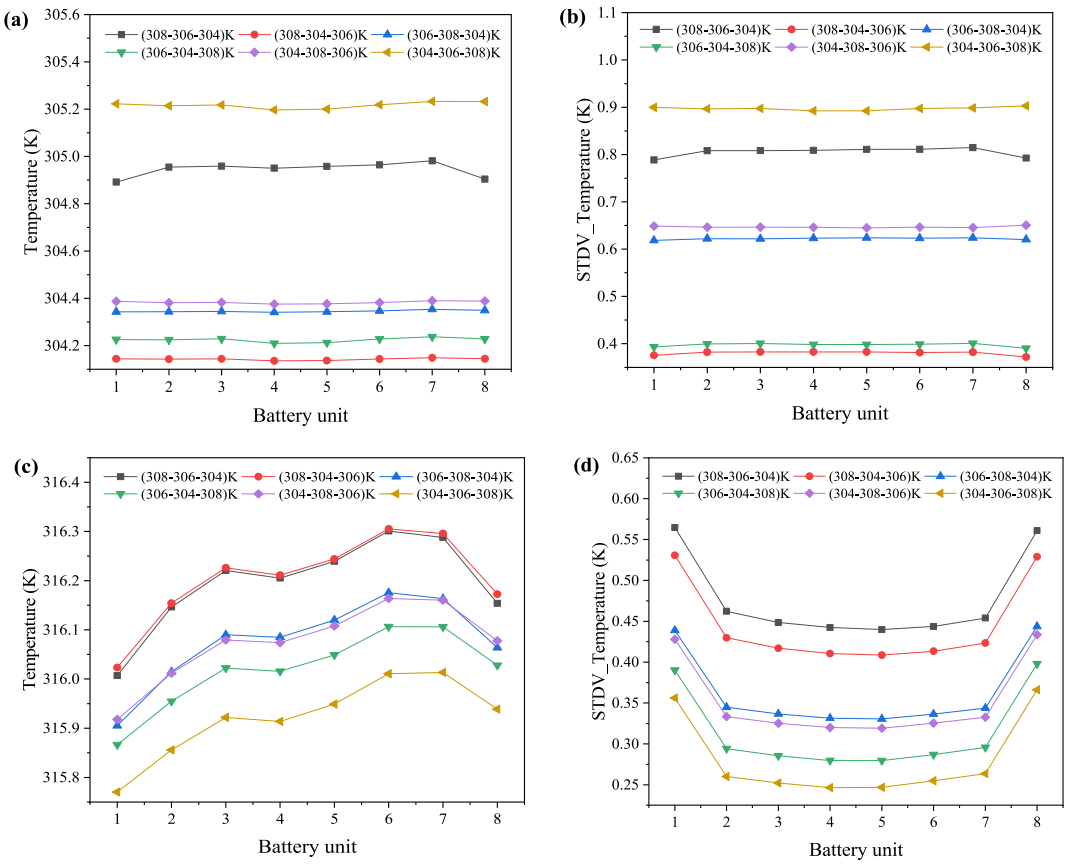

Fig. 6. Maximum temperature rise and STDV of the temperature field for the individual cells at 600 s (a, b), and 3600 s (c, d) under latent heat of 165 kJ/kg, and v = 0.124 m/s.

the subsequent sections.

4.4. Thermal performance of PCMs volume fraction

In this section, we assess the thermal behavior of the proposed BTM based on PCMs volume fraction. The volume fraction is considered according to the height of the heatsink (see Table 4), in which the height is divided into three unequal sections and filled with three different PCMs. A similar approach has been investigated for thermocline thermal energy storage (TES) tank in our previous work [45].

Design DIV is employed and the air inlet velocity and temperature were considered as 0.124 m/s and 300 K, respectively. Fig. 8 (a) and (c) illustrated the maximum temperature of the individual battery units at 600 s and 3600 s, respectively for the different cases studied. At early discharge stage, Case III portrayed the lowest temperature rise among the four cases with the maximum temperature of 303.751 K.

On the other hand, Case IV depicted a higher temperature rise with a maximum temperature recorded as 304.958 K as shown in Fig. 8 (a). Case I and II exhibited mild temperature rise with maximum temperature of 304.293 K and 304.296 K, respectively. The temperature outlines of each of the individual case displayed almost straight lines indicating that, the thermal behavior within the individual battery units as well as the air flow rate within the nine channels were equal (Fig. 8 (a)). However, as the discharge period prolonged, Case IV demonstrated the lowest temperature rise with a value of 312.876 K, while Case III showed the highest temperature upsurge with a value of 315.429 K, as shown in Fig. 8 (c). These results are attributed to the PCM with lower melting temperature at the midsection of the battery module during early discharge, and the PCM with higher melting point at the adjacent of the air outlet regions when the discharge is prolonged, respectively. Contrary to the temperature outlines in Fig. 8 (a), the inner battery units (i.e. battery units 2 to 7) exhibited higher temperature rise than the sided battery units (i.e. battery units 1 and 8) as shown in Fig. 8 (c). This can be related to the absence of surplus heat from the sides of the corner cells (battery units I and 8).

Likewise, for the temperature uniformity, the corresponding STDV at 600 s and 3600 s are illustrated in Fig. 8 (b) and (d), respectively. Case III, which illustrated a lower temperature rise at 600 s, similarly provided a more even temperature distribution among the remaining three cases. It essentially improved the temperature uniformity in the battery module by 10.5%, 17.8%, and 46.3% compared to Case II, I, and IV, respectively, as shown in Fig. 8 (b).

Nevertheless, Case I which exhibited second best thermal performance in term of low temperature rise at 3600 s demonstrated better temperature uniformity among the four cases. It remarkably improved the temperature uniformity in the module by averagely 28.3%, 41.4%, and 63.0%, when compared with Case II, III, and IV, respectively.

5. Conclusions

With the aims of controlling the temperature rise and providing even temperature distribution in the battery pack, a mini heat sink integrated with multiple PCMs and air channels is proposed in this study. The height of the heat sink is divided into three sections and filled with different PCMs. The thermal performance and temperature homogenization of the proposed BTM system under various conditions were investigated. The conclusion remarks are thus drawn as follows:

1. Increasing the air inlet velocity has less effect in mitigating the maximum temperature upsurge at early discharge stage, but improved significantly as the discharge prolonged to 3600 s. Likewise, the temperature difference was minimized with increasing the

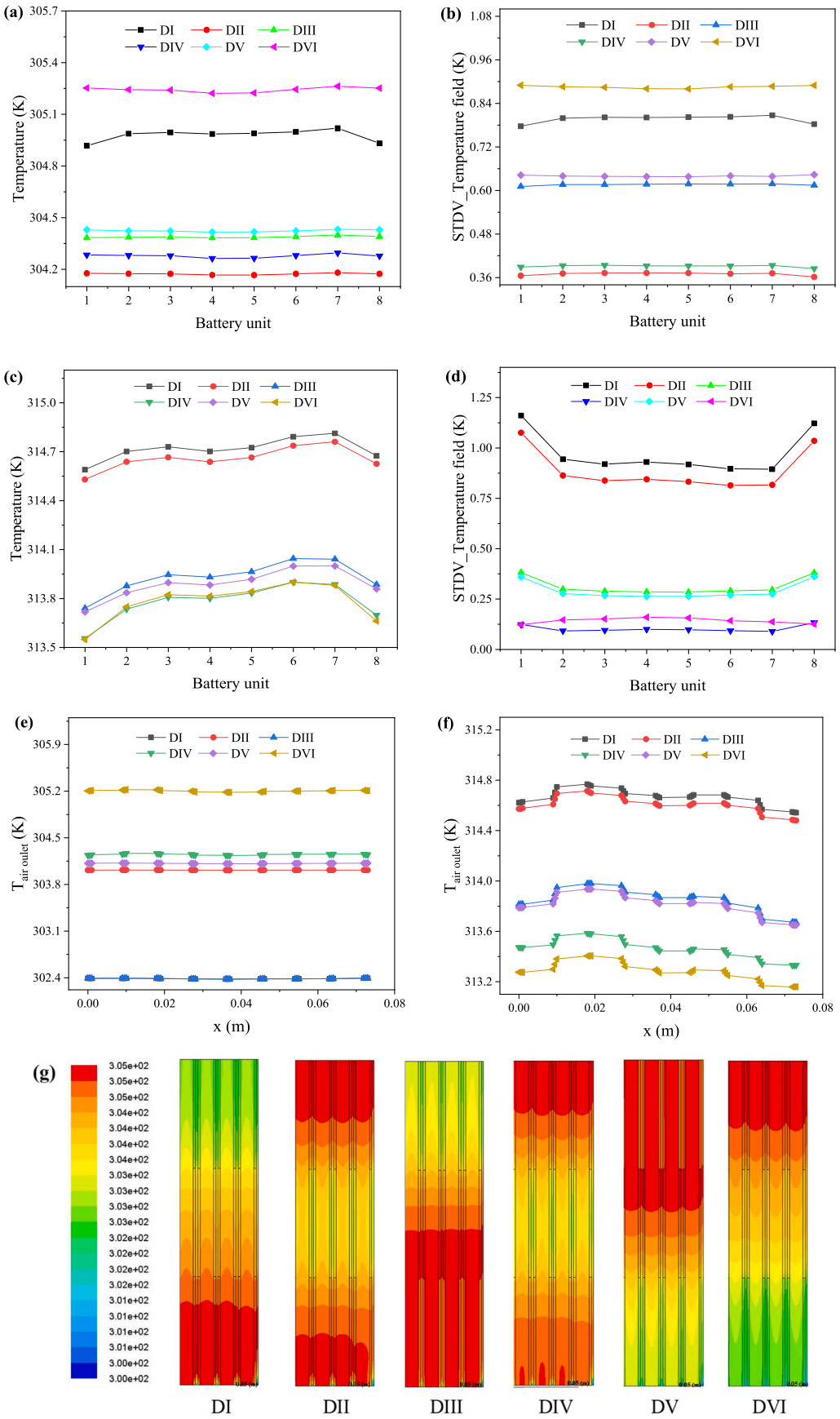

Fig. 7. Maximum temperature values at (a) 600 s, and (c) 3600 s. STDV of the temperature field within the individual battery units at (b) 600 s, and (d) 3600 s. Air outlet temperature at (e) 600 s, and (f) 3600 s. Contour of temperature at (g) 600 s.

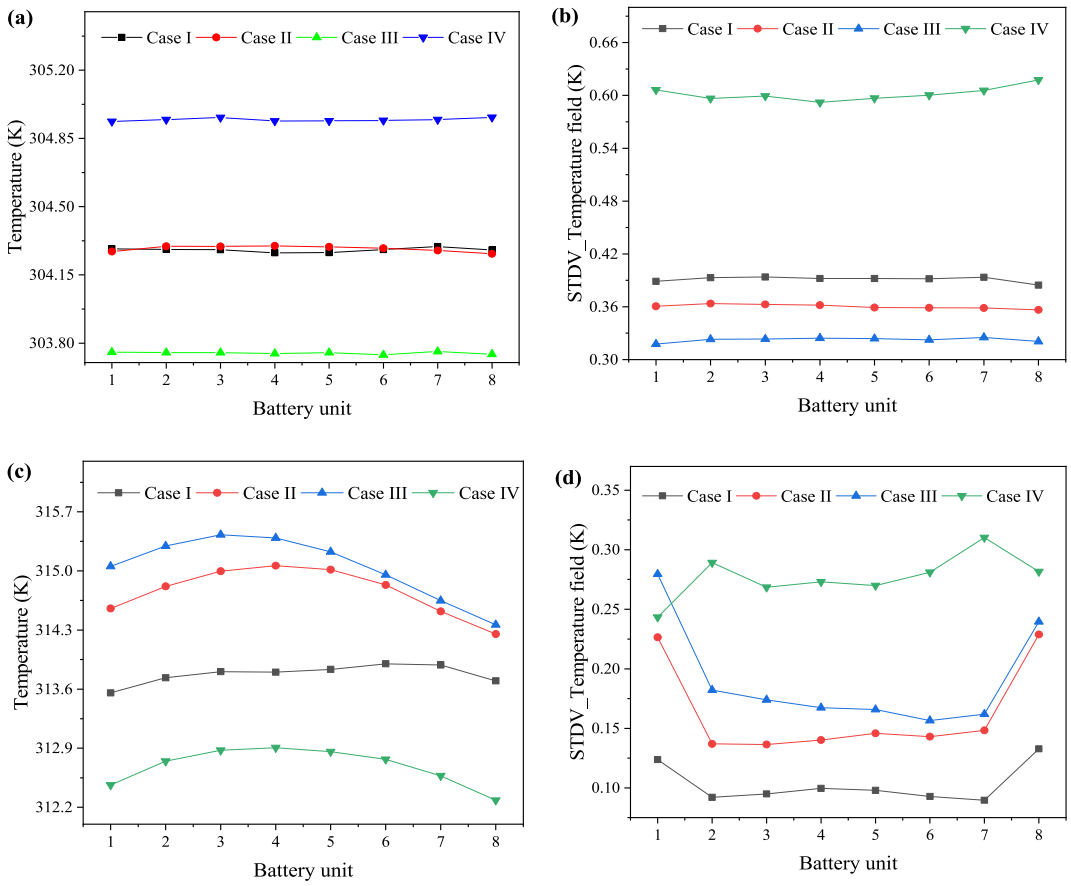

Fig. 8. Evolution of maximum temperature at (a) 600 s, and (c) 3600 s, STDV of temperature field within the individual battery units at (b) 600 s, and (d) 3600 s for different cases studied.

inlet velocity as of T_{core} - T_{te}, but was found to increase as of $T_{core} - T_{be}$ incident.

2. For constant T_{melt} and varying latent heat, the configuration with lower latent heat at the bottom and higher latent heat at the top regions exhibited the least temperature rise and provided better temperature uniformity at 600 s. However, at 3600 s, the configuration with higher latent heat at the midsection of the battery module demonstrated lower temperature rise compared to the remaining configurations.
3. For constant latent heat and varying T_{melt}, the PCMs arrangement having lower melting point at the midsection displayed lower temperature rise and even temperature distribution than the remaining PCMs arrangements at 600 s. In contrast, the arrangement with the higher melting temperature at the outlet region provided a lower temperature profile after 3600 s.
4. For the design of different PCMs arrangement, design DII outperformed the remaining designs by lowering the temperature of the battery module and providing homogenised temperature distribution followed by design DIV at 600 s. However, after 3600 s, design DIV exhibited a better thermal performance and temperature uniformity and can thus be the best choice for a thermal designer.
5. For the case of PCMs volume fraction, Case III illustrated the best thermal performance at early discharge stage while, Case IV depicted the worst. However, after a longer time of discharge, Case IV exhibited the lowest temperature rise but with the least temperature uniformity among the four cases.

CRediT authorship contribution statement

Abubakar Gambo Mohammed: Writing – original draft, Methodology, Software. **Karem Elsayed Elfeky:** Writing – review & editing, Data curation, Supervision. **Qiuwang Wang:** Writing – review & editing, Supervision, Funding acquisition.

Declaration of competing interest

The authors declare that they have no known competing financial interests or personal relationships that could have appeared to influence the work reported in this paper.

Acknowledgement

This work is financially supported by the National Natural Science Foundation of China (Grant No. 51536007), the National Natural Science Foundation of China (NSFC)/Research Grants Council (RGC) Joint Research Scheme (Grant No. 51861165105), the Foundation for Innovative Research Groups of the National Natural Science Foundation of China (No.51721004) the 111 Project (B16038), and the Fundamental Scientific Research Expenses of Xi'an Jiaotong University (xzy012021021).

References

[1] Bp, Statistical Review of World Energy, 2019.
[2] P.H. Andersen, J.A. Mathews, M. Rask, Integrating private transport into renewable energy policy: the strategy of creating intelligent recharging grids for electric vehicles, Energy Pol. 37 (2009) 2481–2486.
[3] Z. Rao, S. Wang, A review of power battery thermal energy management, Renew. Sustain. Energy Rev. 15 (2011) 4554–4571.
[4] G. Zubi, R. Dufo-López, M. Carvalho, G. Pasaoglu, The lithium-ion battery: state of the art and future perspectives, Renew. Sustain. Energy Rev. 89 (2018) 292–308.
[5] K. Amine, J. Liu, I. Belharouak, High-temperature storage and cycling of C-LiFePO4/graphite Li-ion cells, Electrochem. Commun. 7 (2005) 669–673.

[6] P. Ramadass, B. Haran, R. White, B.N. Popov, Capacity fade of Sony 18650 cells cycled at elevated temperatures: Part II. Capacity fade analysis, J. Power Sources 112 (2002) 614–620.
[7] J. Shim, R. Kostecki, T. Richardson, X. Song, K.A. Striebel, Electrochemical analysis for cycle performance and capacity fading of a lithium-ion battery cycled at elevated temperature, J. Power Sources 112 (2002) 222–230.
[8] A.A. Pesaran, Battery thermal models for hybrid vehicle simulations, J. Power Sources 110 (2002) 377–382.
[9] N. Sato, Thermal behavior analysis of lithium-ion batteries for electric and hybrid vehicles, J. Power Sources 99 (2001) 70–77.
[10] T.-H. Tran, S. Harmand, B. Sahut, Experimental investigation on heat pipe cooling for Hybrid Electric Vehicle and Electric Vehicle lithium-ion battery, J. Power Sources 265 (2014) 262–272.
[11] Y. Chen, J. Evans, Heat transfer phenomena in lithium/polyme' electrolyte batteries for electric vehicle application, J. Electrochem. Soc. 140 (1993) 1833–1838.
[12] H. Behi, D. Karimi, M. Behi, M. Ghanbarpour, J. Jaguemont, M.A. Sokkeh, F. H. Gandoman, M. Berecibar, J. Van Mierlo, A new concept of thermal management system in Li-ion battery using air cooling and heat pipe for electric vehicles, Appl. Therm. Eng. 174 (2020), 115280.
[13] K. Chen, Z. Li, Y. Chen, S. Long, J. Hou, M. Song, S. Wang, Design of parallel air-cooled battery thermal management system through numerical study, Energies 10 (2017) 1677.
[14] K. Chen, W. Wu, F. Yuan, L. Chen, S. Wang, Cooling efficiency improvement of air-cooled battery thermal management system through designing the flow pattern, Energy 167 (2019) 781–790.
[15] A.A. Pesaran, Battery thermal management in EVs and HEVs: issues and solutions, in: Proceedings of the Advanced Automotive Battery Conference, Las Vegas, Nevada, 2001.
[16] T. Wang, K.J. Tseng, J. Zhao, Development of efficient air-cooling strategies for lithium-ion battery module based on empirical heat source model, Appl. Therm. Eng. 90 (2015) 521–529.
[17] A. Jarrett, I.Y. Kim, Design optimization of electric vehicle battery cooling plates for thermal performance, J. Power Sources 196 (2011) 10359–10368.
[18] G. Karimi, A. Dehghan, Thermal analysis of high-power lithium-ion battery packs using flow network approach, Int. J. Energy Res. 38 (2014) 1793–1811.
[19] S. Park, D. Jung, Battery cell arrangement and heat transfer fluid effects on the parasitic power consumption and the cell temperature distribution in a hybrid electric vehicle, J. Power Sources 227 (2013) 191–198.
[20] Q. Wang, B. Jiang, B. Li, Y. Yan, A critical review of thermal management models and solutions of lithium-ion batteries for the development of pure electric vehicles, Renew. Sustain. Energy Rev. 64 (2016) 106–128.
[21] X. Yang, Y.Y. Yan, D. Mullen, Recent developments of lightweight, high performance heat pipes, Appl. Therm. Eng. 33–34 (2012) 1–14.
[22] V. Barantsevich, V. Shabalkin, Heat pipes for thermal control of ISS solar battery drive, Appl. Therm. Eng. 23 (2003) 1119–1123.
[23] G. Burban, V. Ayel, A. Alexandre, P. Lagonotte, Y. Bertin, C. Romestant, Experimental investigation of a pulsating heat pipe for hybrid vehicle applications, Appl. Therm. Eng. 50 (2013) 94–103.
[24] Z. Rao, Y. Huo, X. Liu, Experimental study of an OHP-cooled thermal management system for electric vehicle power battery, Exp. Therm. Fluid Sci. 57 (2014) 20–26.
[25] J. Wang, Y. Gan, J. Liang, M. Tan, Y. Li, Sensitivity analysis of factors influencing a heat pipe-based thermal management system for a battery module with cylindrical cells, Appl. Therm. Eng. 151 (2019) 475–485.
[26] S. Al Hallaj, J.R. Selman, A novel thermal management system for electric vehicle batteries using phase-change material, J. Electrochem. Soc. 147 (2000) 3231–3236.
[27] X. Duan, G.F. Naterer, Heat transfer in phase change materials for thermal management of electric vehicle battery modules, Int. J. Heat Mass Tran. 53 (2010) 5176–5182.
[28] N. Javani, I. Dincer, G.F. Naterer, G.L. Rohrauer, Modeling of passive thermal management for electric vehicle battery packs with PCM between cells, Appl. Therm. Eng. 73 (2014) 307–316.
[29] R. Kizilel, A. Lateef, R. Sabbah, M.M. Farid, J.R. Selman, S. Al-Hallaj, Passive control of temperature excursion and uniformity in high-energy Li-ion battery packs at high current and ambient temperature, J. Power Sources 183 (2008) 370–375.
[30] M. Nofal, S. Al-Hallaj, Y. Pan, Thermal management of lithium-ion battery cells using 3D printed phase change composites, Appl. Therm. Eng. 171 (2020), 115126.
[31] Y.-H. Huang, W.-L. Cheng, R. Zhao, Thermal management of Li-ion battery pack with the application of flexible form-stable composite phase change materials, Energy Convers. Manag. 182 (2019) 9–20.
[32] W. Wu, G. Zhang, X. Ke, X. Yang, Z. Wang, C. Liu, Preparation and thermal conductivity enhancement of composite phase change materials for electronic thermal management, Energy Convers. Manag. 101 (2015) 278–284.
[33] D. Zou, X. Liu, R. He, S. Zhu, J. Bao, J. Guo, Z. Hu, B. Wang, Preparation of a novel composite phase change material (PCM) and its locally enhanced heat transfer for power battery module, Energy Convers. Manag. 180 (2019) 1196–1202.
[34] A. Lazrak, J.-F. Fourmigué, J.-F. Robin, An innovative practical battery thermal management system based on phase change materials: numerical and experimental investigations, Appl. Therm. Eng. 128 (2018) 20–32.
[35] M. Pan, Y. Zhong, Experimental and numerical investigation of a thermal management system for a Li-ion battery pack using cutting copper fiber sintered skeleton/paraffin composite phase change materials, Int. J. Heat Mass Tran. 126 (2018) 531–543.
[36] C. Wang, T. Lin, N. Li, H. Zheng, Heat transfer enhancement of phase change composite material: copper foam/paraffin, Renew. Energy 96 (2016) 960–965.
[37] Z. Ling, F. Wang, X. Fang, X. Gao, Z. Zhang, A hybrid thermal management system for lithium ion batteries combining phase change materials with forced-air cooling, Appl. Energy 148 (2015) 403–409.
[38] M.Y. Ramandi, I. Dincer, G.F. Naterer, Heat transfer and thermal management of electric vehicle batteries with phase change materials, Heat Mass Tran. 47 (2011) 777–788.
[39] S. Al-Hallaj, G. Albright, Energy storage thermal management system using multi-temperature phase change materials, in: US Patent Application Publication, All Cell Technologies, LLC, Chicago, US, 2012. PCT/US2012/041361.
[40] C. Lin, Y. Sun, Z. Li, S. Xu, Simulation and Parametric Analysis of Battery Thermal Management System Using Phase Change Material, SAE International, 2020.
[41] J. Zhao, C. Wu, Z. Rao, Investigation on the cooling and temperature uniformity of power battery pack based on gradient phase change materials embedded thin heat sinks, Appl. Therm. Eng. 174 (2020), 115304.
[42] L. Fan, J.M. Khodadadi, A.A. Pesaran, A parametric study on thermal management of an air-cooled lithium-ion battery module for plug-in hybrid electric vehicles, J. Power Sources 238 (2013) 301–312.
[43] Z. Rao, S. Wang, G. Zhang, Simulation and experiment of thermal energy management with phase change material for ageing LiFePO4 power battery, Energy Convers. Manag. 52 (2011) 3408–3414.
[44] www.rubitherm.com.
[45] K.E. Elfeky, A.G. Mohammed, N. Ahmed, L. Lu, Q. Wang, Thermal and economic evaluation of phase change material volume fraction for thermocline tank used in concentrating solar power plants, Appl. Energy 267 (2020), 115054.